time integration scheme.

In the normal direction, the normal stress is related to the normal displacement which is governed by the cavity nucleation, growth, and coalescence on the grain boundary. Substituting Eqs. (9), (10), (12) and (13) into Eq. (8), the normal displacement rate can be expressed as a function of the normal stress in a quadratic form, such that

$$\Delta\dot{u}_n = A\sigma_n^2 + B\sigma_n + C \tag{16}$$

where

$$A = \frac{V}{\pi b^2}\frac{1}{N}\frac{F_n}{\Sigma_0^2}\dot{\varepsilon}_e^c \tag{17a}$$

$$B = \frac{1}{\pi b^2}\frac{4\pi D}{\ln(\frac{1}{f}) - \frac{1}{2}(3-f)(1-f)} \tag{17b}$$

$$C = \frac{\dot{V}_2}{\pi b^2} - \frac{V}{\pi b^2}(\dot{\varepsilon}_I + \dot{\varepsilon}_{II}) \tag{17c}$$

It is worth noting that *A*, *B*, and *C* signify, respectively, the contributions of cavity nucleation, atom diffusion, and creep to the normal separation.

The material tangent with respect to the incremental normal displacement can be derived from Eq. (16):

$$\frac{\partial\Delta\sigma_n}{\partial\Delta u_n} = \frac{1}{(2A\sigma_n + B)\Delta t} \tag{18}$$

Combining Eqs. (15) and (18), the material Jacobian (tangent stiffness) matrix can be obtained, such that

$$\begin{Bmatrix}\Delta\sigma_n \\ \Delta\tau\end{Bmatrix} = \begin{bmatrix}\frac{1}{(2A\sigma_n + B)\Delta t} & 0 \\ 0 & \frac{\eta}{w\Delta t}\end{bmatrix}\begin{Bmatrix}\Delta u_n \\ \Delta u_s\end{Bmatrix} \tag{19}$$

All components in the material Jacobian matrix are derived in an explicit integration scheme and are implemented in the user subroutine UEL in ABAQUS.

Since the creep information of the grain element should be gathered from adjacent grain elements for the grain boundary element, it is necessary to access the information of state variables, including the stress state and the effective creep strain rate. A user-defined material (UMAT) for power law creep is implemented accordingly. By a special ordering of elements and a common block, all the information can be accessed effectively.

4. Numerical examples

All the parameters in simulation are normalized by the initial grain facet length R_i, Young's Modulus of grain element E and the applied strain rate $\dot{\varepsilon}_{app}$. The facet length is set to 1 μm at initial, Young's modulus is 500 GPa and Poisson's ration ν is 0.129 for grain elements. The reference stress σ_0 is $0.001E$, the reference strain rate $\dot{\varepsilon}_0$ is 1.0 and the order n is 5 for power law creep in grain elements.

For a grain boundary element, the initial void radius a is set to be $0.67\times10^{-3}R_i$ and the half void spacing b is $0.67R_i$. The initial reference density of the undeformed grain boundary N_R is $1/\sqrt{\pi R_i}$, and the initial density of the undeformed grain boundary N_i is $40N_R$. The material parameter F_n in a nucleation law is set to $5.4\times10^4 N_R$ for brittle material, and the reference stress Σ_0 is $0.01E$. The viscosity η^* is normalized by the applied strain rate $\dot{\varepsilon}_{app}$ and Young's modulus E:

$$\eta^* = \frac{\eta_b\dot{\varepsilon}_{app}}{E} = 5\times10^3 \tag{20}$$

The normalized diffusion parameter D^* is determined by

$$D^* = \frac{DE}{\dot{\varepsilon}_{app}R_i^3} = 10^{-5} \tag{21}$$

For all the time scale, t is normalized by applied strain rate $t^* = t\dot{\varepsilon}_{app}$ and all the length scale are normalized by R_i.

4.2 Model verification: a bi-crystal model

The first example is a simple bi-crystal that consists of two square gains with a facet length of R_i and a single grain boundary as depicted in Fig. 3 [11, 12]. This example is conducted to verify the accuracy of current model. Specifically, the two grains are modelled by the plane strain element (CPE4 in ABAQUS) and the grain boundary is modelled using the rate-dependent cohesive element developed herein. The bi-crystal model is loaded by a constant displacement distributed along the top and bottom edges, while the transverse degree of freedom (in the

x-direction) of each node is constrained. The applied strain rate is set to meet the stead state creep strain rate. The initial normalized time step t^* is set at 10^{-9} and the following time steps are adjusted automatically by ABAQUS to meet the desirable convergence with efficiency.

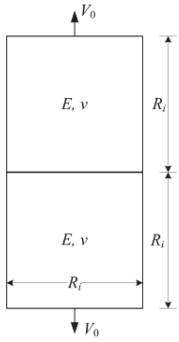

Fig. 3 Bi-crystal with simple boundary value problem

To verify the accuracy, a direct integration form updated by an analytical solution has been computed via a MATLAB code and the results are compared with those obtained from the finite element analysis.

Figures 4 (b)-4(d) show the relationship of the void radius *a*, void spacing *b*, and *a*/*b* as functions of time. In Fig. 4(b), the increase of the void radius, *a*, with time represents the growth of the void on the grain boundary. It indicates that the cavity growth remains almost the same for different nucleation rates before fracture. On the other hand, the void spacing, *b*, decreases faster with time which indicates more cavity nucleation occurs before fracture.

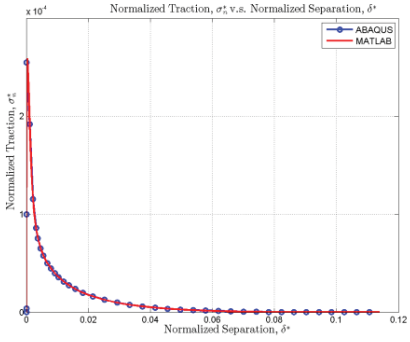

Fig. 4(a) Normalized traction-separation relation with different nucleation rates.

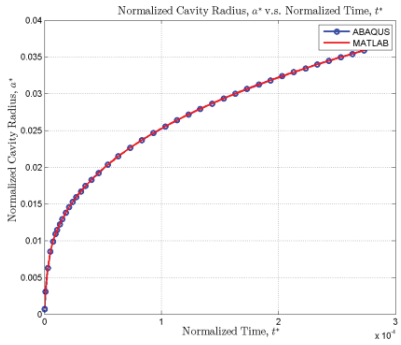

Fig. 4(b) Normalized void radius *a* v.s. Normalized time t^* with different nucleation rates.

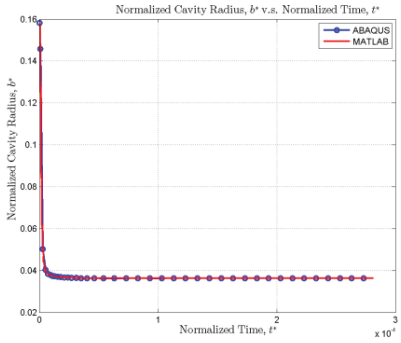

Fig 4(c) Normalized void spacing b^* v.s. normalized time t^* with different nucleation rates.

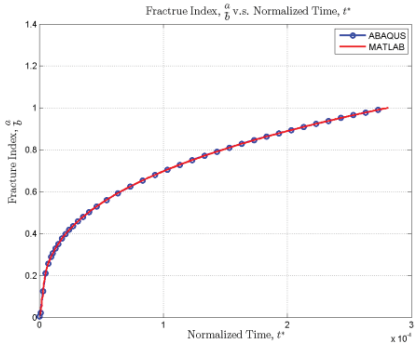

Fig 4(d) *a*/*b* ratio v.s normalized time t^* with different nucleation rates.

We noted that *b* attains a minimum and remains almost constantly at the final stage of fracture. This is because the nucleation rate is also influenced by effective creep rate and when the normal traction reaches its limit, the effective strain rate dropped quickly. Finally, the ratio of *a* to *b* increases monotonically and reaches the upper limit of 1.0 which represents complete separation of the grain

boundary.

4.2. Polycrystalline ZrB_2-SiC composites

A polycrystal model is conducted to study the creep fracture of the zirconium diboride (ZrB_2) and silicon carbide (SiC) composite. A configuration of polycrystalline grains is shown in Fig. 6. For the sake of convergence, the facet length of each grain boundaries is equally discretized with 500 nm cohesive elements. Each grain is constructed by numbers of three-node triangle plane strain elements (CPE3 element in ABAQUS). In our study, each grain boundary element is attached to two adjacent grain elements. Material properties adopted are the same as those used in the previous bi-crystal example. The model is subjected to a constant tension of 75 MPa, while the horizontal degree of freedom at the right and the left boundaries is fixed.

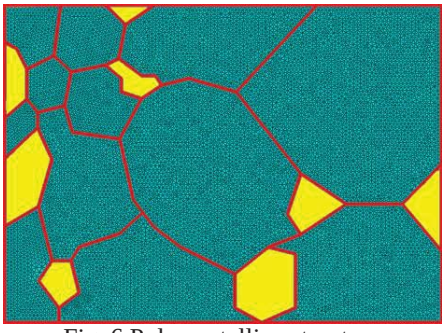

Fig. 6 Polycrystalline structure

Because of the composites of ceramics, such as the SiC-ZrB_2, there exists different properties on the grain boundary due to impurities [13]. The cavity nucleation ability is only allowed at the grain boundaries between ZrB_2 and SiC grains. Figure 7 shows the von-Mises stress contour and crack pattern for polycrystalline grains at high temperatures. We observe that there exists a severe stress concentration at the triple junction between ZrB_2 and SiC grains. This stress heterogeneity phenomenon agrees with the experimental observation [14]. This phenomenon is a direct consequence of the nucleation properties assigned at the ZrB_2-SiC grain boundaries.

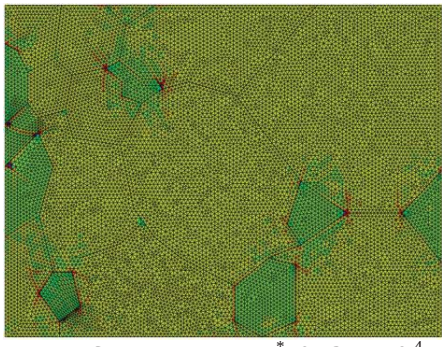

Fig. 7 Stress contour at $t^*=0.1325\times10^{-4}$

5. Conclusions

A robust rate-dependent cohesive element has been developed and implemented in ABAQUS. The model presented here accounts for the fracture mechanisms in microstructures, i.e., viscous grain boundary sliding, the nucleation of grain boundary cavities, their growth by grain boundary diffusion and local creep, and link up of microcracks to form macrocracks. The bicrystal verification confirms the robustness and stabilities of the implementation. The method is also used to study the creep fracture of ultra-high temperature ceramics composites. The results indicate there exists a stress heterogeneity due to a different grain boundary properties. This presence of heterogeneity predicted by the simulation agrees with experimental observations.

Acknowledgements

The research was performed under the finical support by National Science Council, Taiwan. The authors would like to express their gratitude to Simutech Solution Corp. Taiwan for providing computational support. We are also grateful to the National Center for High-Performance Computing for providing the computational resources. Finally, we would also like to express our sincere gratitude to Marc Bird, Professors Ken White and P. Sharma (University of Houston) and P. F. Becher (University of Tennessee) for their enlightening comments and discussions.

References

[1]G. D. Quinn, "Fracture mechanism maps for advanced structural ceramics - Part 1 Methodology and hot-pressed silicon nitride

results," *Journal of Materials Science,* vol. 25, pp. 4361-4376, 1990.
[2]G. D. Quinn and W. R. Braue, "Fracture mechanism maps for advanced structural ceramics - Part 2 Sintered silicon nitride," *Journal of Materials Science,* vol. 25, pp. 4377-4392, 1990.
[3] C. H. Hsueh and A. G. Evans, "Overview 14 Creep fracture in ceramic polycrystals-II. effects of inhomogeneity on creep rupture," *Acta Metallurgica,* vol. 29, pp. 1907-1917, 1981.
[4] A. F. Bower, *Aplied Mechanics of Solids*: Taylor & Francis Group, LLC, 2010.
[5] M. F. Ashby, "Boundary Defects, and Atomistic Aspects of Boundary Sliding and Diffusional Creep," *Surface Science,* vol. 31, pp. 498-&, 1972.
[6] J. R. Rice, "Constraints on the Diffusive Cavitation of Isolated Grain-Boundary Facets in Creeping Polycrystals," *Acta Metallurgica,* vol. 29, pp. 675-681, 1981.
[7] P. Onck and E. Van Der Giessen, "Growth of an initially sharp crack by grain boundary cavitation," *Journal of the Mechanics and Physics of Solids,* vol. 47, pp. 99-139, 1998.
[8] E. Van Der Giessen and V. Tvergaard, "Development of final creep failure in polycrystalline aggregates," *Acta Metallurgica Et Materialia,* vol. 42, pp. 959-973, 1994.
[9] A. Needleman and J. R. Rice, "Plastic creep flow effects in the diffusive cavitation of grain boundaries," *Acta Metallurgica,* vol. 28, pp. 1315-1332, 1980.
[10] C.-H. Yu, C.-W. Huang, C.-S. Chen, Y. Gao, and C.-H. Hsueh, "Effects of Grain Boundary Heterogeneities on Creep Fracture of Ultra-High Temperature Ceramics," presented at the 6th European Congress on Computational Methods in Applied Sciences and Engineering, Vienna, Austria, 2012.
[11] Simulia, "ABAQUS," 6.10 ed. Pawtucket, Rhode Island, 2010.
[12] Y. F. Gao and A. F. Bower, "A simple technique for avoiding convergence problems in finite element simulations of crack nucleation and growth on cohesive interfaces," *Modelling and Simulation in Materials Science and Engineering,* vol. 12, pp. 453-463, May 2004.
[13] C.-H. Yu, C.-W. Huang, C.-S. Chen, Y. Gao, and C.-H. Hsueh, "A micromechanics study of competing mechanisms for creep fracture of zirconium diboride polycrystals," *Journal of the European Ceramic Society,* vol. 33, pp. 1625-1637, 2013.
[14] M. W. Bird, R. P. Aune, A. F. Thomas, P. F. Becher, and K. W. White, "Temperature-dependent mechanical and long crack behavior of zirconium diboride-silicon carbide composite," *Journal of the European Ceramic Society,* 2012.